Mon. Not. R. Astron. Soc. **000**, 000–000 (0000) Printed February 5, 2008 (MN LATEX style file v1.4)

Weighing black holes with warm absorbers

R. Morales⋆ and A. C. Fabian
Institute of Astronomy, Madingley Road, Cambridge CB3 0HA

February 5, 2008

ABSTRACT
We present a new technique for determining an upper limit for the mass of the black hole in active galactic nuclei showing warm absorption features. The method relies on the balance of radiative and gravitational forces acting on outflowing warm absorber clouds. It has been applied to 6 objects: five Seyfert 1 galaxies: IC 4329a, MCG−6-30-15, NGC 3516, NGC 4051 and NGC 5548; and one radio-quiet quasar: MR 2251-178. We discuss our result in comparison with other methods. The procedure could also be applied to any other radiatively driven optically thin outflow in which the spectral band covering the major absorption is directly observed.

Key words: galaxies: active − galaxies: Seyfert − X-rays: galaxies.

1 INTRODUCTION

It is the current paradigm that the fundamental power source of all Active Galactic Nuclei (AGN) is accretion onto a supermassive black hole (SMBH) (see Lynden-Bell 1969 and Rees 1984). For many years, theorists and observers have attempted to prove the existence of SMBHs, inferring their presence by studying how they affect the surrounding environment (Kormendy & Richstone 1995 and Richstone et al. 1998 review the SMBH search). A variety of techniques and arguments has been developed to estimate the mass of the central engine in AGN (Ho & Kormendy 2000). This has included both theoretical and observational methods such as: fitting the spectra of accretion discs; high efficiency and Eddington limit arguments; stellar dynamical searches; kinematics of radio masers; X-ray variability and virial masses from optical variability, which includes reverberation mapping and photoionization model techniques.

In this paper we propose the use of warm absorbers (WAs) to determine an upper limit to the BH mass. WAs are significant quantities of partially-ionized, optically-thin material found mainly in the vicinity of Type 1 Seyfert galaxies. This gas is most readily observable when it lies along line-of-sight to the central X-ray source: the observed X-ray spectrum then displays well-defined K-shell absorption edges. Halpern (1984) was the first to postulate the presence of such material based on the unusual X-ray spectrum of the QSO MR 2251-178 from the *Einstein* observatory. The clearest demonstration of the presence of warm absorbing material comes from spectroscopic observations of the OVII and OVIII K-shell absorption edges at 0.74 and 0.87 keV, respectively. These edges were first found by the *ROSAT* PSPC (Nandra & Pounds 1992). The spectral capabilities of *ASCA* allowed for detailed studies of such edges (e.g. Fabian et al. 1994, Otani et al. 1996, Brandt et al. 1996, Mathur et al. 1997, Reynolds 1997, Leighly et al. 1997 and George et al. 1998). WAs are common, being detected in half of the sources (Reynolds 1997, George et al. 1998). Several different models have been suggested concerning the nature and location of the WA. Among others, these include the very detailed studies by Krolik & Kriss (1995) and Netzer (1996). The reason for the large variety of models is that not all physical properties of the WA can be directly determined from X-ray spectral fits, but only certain combinations of them.

In addition to the WAs, associated UV and optical absorption features are also typically found in AGN spectra (see Crenshaw et al. 1999 and references therein for an overview). A common property shared by almost all associated absorption features is that any velocity shift is always to the *blue* of the systemic velocity, implying that the absorbing material is outflowing. Crenshaw et al. (1999) found a one-to-one correspondence between those objects showing UV absorption and those presenting X-ray WAs. This implies the two phenomena are likely to be physically related. However, since WAs generally reveal higher ionization states, and higher column densities, they can not be the same in general. A very plausible connection is a dynamical one in which both UV absorbers and X-ray WAs are outflowing. The blue-shifts in X-ray absorption lines have recently been revealed by *Chandra* observations (e.g. Kaastra et al. 2000, Kaspi et al. 2000, Collinge et al. 2001), presenting typical velocities of several hundred to several thousand km s^{-1}. One unresolved issue is whether the outflowing gas is smoothly distributed (i.e. winds) or resides in discrete clouds. Krolik & Kriss (1995) show that the warm absorption seen in many

⋆ E-mail: rm@ast.cam.ac.uk

X-ray spectra of AGN may be produced by X-ray heated winds. Reynolds & Fabian (1995) also sketch some ideas relating the WA to a radiatively driven outflow. In contrast to the wind model, Chelouche & Netzer (2001) show that accelerations to velocities of a few hundred to a few thousand $\mathrm{km\ s^{-1}}$ is a natural consequence of the AGN environment when radiation pressure acts on external pressure-confined highly ionized clouds (responsible for the WA features). For the present study, we will adopt the latter model in which WA clouds are radiatively accelerated by the central ionizing continuum.

This work describes a new method for obtaining an upper limit on an AGN BH mass, by means of a comparison between the radiative and gravitational forces acting on its WA clouds. Section 2 presents the 30 observations of the 6 AGNs sample to which our technique has been applied. The description of our method, a spectral analysis of the *ASCA* data and the results and comparison with other BH mass estimates by different techniques are addressed in Section 3. Section 4 and 5 analyse the influence of the underlying continuum on our estimate and further terms in the equation of motion, respectively. Finally, in Section 6 our conclusions are summarized. Throughout this paper, unless otherwise stated, errors on physical quantities are quoted at the 1σ level for one interesting parameter.

2 THE DATA

We have studied a sample of six AGNs consisting of five Seyfert 1 galaxies (IC 4329a, MCG−6-30-15, NGC 3516, NGC 4051 and NGC 5548) and one radio-quiet quasar (MR 2251-178), which cover a range of almost 4 orders of magnitude in X-ray luminosity. These objects are a subsample of those presenting warm absorption features in the 24 Type 1 AGN sample of Reynolds (1997). With the exception of MR 2251-178, the other five Seyfert galaxies are also present in the George et al. (1998) survey. The WAs of all these sources have a very rich observational history (Komossa 1999) and their host AGNs are amongst the brightest ones in the nearby Universe ($z \geq 0.07$). The spectral files have been downloaded from the Tartarus Database (`http://tartarus.gsfc.nasa.gov/`) and the 30 observations analysed are listed in Table 1.

Source	Type	Redshift z	Galactic N_H (10^{20} cm^{-2})	Date of Observation
IC 4329a	Sy1	0.016	4.55[a]	93/08/15
				97/08/07
				97/08/10
				97/08/12
				97/08/15
MCG−6-30-15	Sy1	0.008	4.06[a]	93/07/09
				93/07/31
				94/07/23
				97/08/03
				97/08/07
MR 2251-178	RQQ	0.068	2.8	93/11/16
				93/12/07
				93/12/14
				93/12/19
				93/12/24
NGC3516	Sy1	0.009	3.4	94/04/02
				95/03/11
				95/03/12
NGC4051	Sy1	0.002	1.31[a]	93/04/25
				94/06/07
NGC5548	Sy1	0.017	1.7	93/07/27
				96/06/27
				96/06/29
				96/07/01
				96/07/03
				96/07/04
				98/06/15
				98/06/20
				98/07/07
				99/01/19

Table 1. The AGN sample. Column 1 gives the common source name. Column 2 indicates the type of nuclear activity (Sy1 ≡ Seyfert 1 galaxy; RQQ ≡ radio-quiet quasar). Column 3 give the redshift of the sources (Veron-Cetty & Veron 1993). Column 4 gives the Galactic HI column density towards the source as determined by 21-cm measurements ["a" indicates an accurate value obtained from Elvis, Wilkes & Lockman (1989); otherwise quoted values are interpolations from the measurements of Stark et al. (1992)]. Column 5 gives the year/month/day of the *ASCA* observation used (see the Tartarus Database for a detailed description of each observation).

3 UPPER BLACK HOLE MASS ESTIMATE

3.1 Description of the method

The following assumptions have been made:

- the WA, responsible for the absorption features around 1 keV , is present in the form of clouds.
- these clouds are pushed radiatively outwards.
- the clouds motion is entirely radial.

The radial equation of motion for these WA clouds is

$$\frac{AL_{\rm abs}}{4\pi r^2 c} - \frac{GM_{\rm BH}m_{\rm wa}}{r^2} - \rho_{\rm o} v^2 A = m_{\rm wa} a \qquad (1)$$

where: A is the cross-section presented by the WA clouds; $L_{\rm abs}$ is the luminosity absorbed by the WA cloud; r is the distance from the ionizing source to the WA cloud; c is the velocity of light; G is the gravitational constant; $M_{\rm BH}$ is the black hole mass; $m_{\rm wa}$ is the mass of a WA cloud; $\rho_{\rm o}$ is the density of the medium through which the WA is moving; v is the velocity of the WA clouds with respect to that medium and a is the acceleration experienced by the WA cloud.

The first term on the left hand side is the outward force due to radiation pressure, the second term is the restoring force due to gravity, and the third term describes any drag force (i.e. ram pressure) experienced by the WA when moving through an intercloud medium. If the drag force and the acceleration term are negligible, a comparison between the

radiation and gravitation terms leads to an expression for the BH mass:

$$M_{\rm BH} = \frac{L_{\rm abs}}{4\pi c G m_{\rm p} N_{\rm wa}} \quad (2)$$

where $m_{\rm p}$ is the proton rest-mass and $N_{\rm wa}$ is the column density of the WA clouds. If these terms are non negligible and positive, then the above expression becomes an upper limit for $M_{\rm BH}$. We shall treat it as such in the rest of the paper and discuss further the drag and acceleration terms in Section 5.

The only two unknowns in Eqn. 2 are $L_{\rm abs}$ and $N_{\rm wa}$. $N_{\rm wa}$ is calculated as a parameter in our spectral fits of a single ionization parameter model presented in the following subsection. As already seen in Reynolds (1997) and George et al. (1998), the data can often be well fit by such a model which allows for accurate estimates of the ionization parameter and column densities. The calculation of L_{abs} has been performed using the fact that the photoionized plasma causing the edges is optically thin along the line of sight. Therefore, the expression for the radiation pressure, $P_{\rm rad}$, can be written as

$$P_{\rm rad} = \frac{L_{\rm abs}}{4\pi r^2 c} = \frac{1}{4\pi c r^2} \int_{\nu_{\rm min}}^{\nu_{\rm max}} (L(\nu) - L_{\rm obs}(\nu)) d\nu \quad (3)$$

where: $L(\nu)$ is the luminosity per unit frequency from the ionizing source (which we assume to be a power law of photon index Γ) and $L_{\rm obs}(\nu)$ is the luminosity per unit frequency observed after $L(\nu)$ has passed through the WA cloud. The photoionization models can predict both the intensity of the incident and transmitted continuum allowing the calculation of the above integral (see Section 3.2.3). We have chosen the limits of our integration to be: $\nu_{\rm min} = 1$ eV and $\nu_{\rm max} = 20$ keV .

3.2 Spectral analysis

The data have been fitted using two different models. The aim for this multiple analysis has been firstly, to determine phenomenologically the underlying continuum by mimicking the WA features by the two photoionization absorption edges at the OVII and OVIII rest-frame energies (Sections 3.2.1 and 3.2.2); and then to calculate the radiation pressure acting on the WA (Section 3.2.3). Data from all four *ASCA* instruments were fitted simultaneously. SIS data between 0.5–4.0 keV and GIS data between 0.8–4.0 keV were used. The spectra were then fitted using the standard χ^2 minimization technique implemented in version 11.0.1 of the XSPEC spectral fitting package (Arnaud 1996).

3.2.1 Phenomenological model

In order to determine the underlying continuum hidden by various spectral features displayed by the data, the spectrum of each object was fitted by a spectral model consisting of the following components:

- a power-law representing the primary continuum (photon index Γ)
- two absorption edges with rest-frame threshold energies of 0.74 keV and 0.87 keV representing OVII and OVIII K-shell absorption (with maximum optical depths $\tau_{\rm O7}$ and $\tau_{\rm O8}$) respectively. These two edges provide, to a good approximation, a description of the effects of the warm absorber over the ASCA band.
- intrinsic absorption by a column density $N_{\rm H}$ of neutral matter in the rest frame of the source. This absorbing material is assumed to have cosmic abundances.
- Galactic absorption (at $z = 0$) fixed at the level determined by the HI 21-cm measurements reported in Table 1, column 4.

Free parameters in the fit were Γ, $\tau_{\rm O7}$, $\tau_{\rm O8}$ and $N_{\rm H}$. The normalizations of the model for each of the four instruments were also left as free parameters. This allows for the known $\sim$ 10–20 per cent discrepancies between the normalizations of different instruments (see `http://heasarc.gsfc.nasa.gov/docs/asca/watchout.html` for a discussion of the decrease in efficiency of SIS0 and SIS1 below 1 keV since approximately late 1994). Table 2 presents a summary of the χ^2 fitting.

As noted in Reynolds (1997), fixing the energies of the two absorption edges at the physical rest-frame energies of the K-shell absorption edges of OVII and OVIII, is the most robust to the various unmodeled spectral complexities such as recombination line/continuum emission, resonance absorption lines and other absorption edges. These complexities would require many additional degrees of freedom to model (such as the covering fraction of the warm material, its density, the chemical abundances and the velocity structure) and would lead to an over modeling of the data for all but the very highest quality *ASCA* data. In fitting a simple two-edge model, these complexities could lead to false shifts in the threshold edge of the edges (e.g. the existence of the Ne IX edge may falsely imply a small blueshift of the OVIII edge when a two-edge model is fitted with the edge threshold energies as free parameters).

3.2.2 Soft excess

A detailed study of the soft excess was not performed since soft excesses are expected to be most noticeable below ~ 0.6 keV . This is the energy below which significant SIS calibration uncertainties exist. However, for completeness and following the analysis in Reynolds (1997), a black-body component (subject to neutral and ionized absorption) was added to the above model and the data were re-fitted. To avoid being severely biased by calibration uncertainties below 0.5 keV , all data below this energy were discarded. The results found are presented in Table 3, where a significant improvement of the fit is obtained for MCG−6-30-15, NGC 3516, NGC 4051, and NGC 5548.

3.2.3 Photoionization models

It will be assumed that the physics of the WA is dominated by photoionization. This assumption results from the very high and variable ionization state. Quantitative evidence for this comes from the observed anti-correlation between the OVIII absorption edge depth and the primary ionizing flux observed during the long observation of MCG−6-30-15 (Otani et al. 1996). Also NGC 4051 has shown variability of the OVII edge (Guainazzi et al. 1996). A grid of self-consistent models has been produced using Ferland's

Source	Date of Observation	Photon index Γ	$\tau_{\rm O7}$	$\tau_{\rm O8}$	Intrinsic $N_{\rm H}$ (10^{22} cm^{-2})	χ^2/dof	Red. χ^2
IC4329a	93/08/15	$1.85^{+0.01}_{-0.01}$	$0.67^{+0.06}_{-0.06}$	$0.06^{+0.04}_{-0.04}$	$0.30^{+0.01}_{-0.01}$	1036.6/776	1.34
	97/08/07	$1.90^{+0.01}_{-0.01}$	$0.11^{+0.07}_{-0.07}$	$0.00^{+0.01}_{-0.00}$	$0.44^{+0.01}_{-0.01}$	1328.5/1007	1.32
	97/08/10	$1.79^{+0.01}_{-0.02}$	$0.45^{+0.06}_{-0.08}$	$0.00^{+0.02}_{-0.00}$	$0.34^{+0.01}_{-0.01}$	825.5/776	1.06
	97/08/12	$1.91^{+0.02}_{-0.02}$	$0.28^{+0.08}_{-0.08}$	$0.00^{+0.02}_{-0.00}$	$0.42^{+0.01}_{-0.01}$	896.2/776	1.15
	97/08/15	$1.91^{+0.02}_{-0.02}$	$0.09^{+0.10}_{-0.10}$	$0.04^{+0.04}_{-0.04}$	$0.47^{+0.02}_{-0.02}$	1308.2/1009	1.30
MCG−6-30-15	93/07/09	$2.01^{+0.01}_{-0.01}$	$0.65^{+0.03}_{-0.03}$	$0.23^{+0.02}_{-0.02}$	$0.00^{+0.00}_{-0.00}$	1203.7/775	1.55
	93/07/31	$1.88^{+0.01}_{-0.01}$	$0.70^{+0.04}_{-0.04}$	$0.49^{+0.03}_{-0.03}$	$0.00^{+0.00}_{-0.00}$	1110.9/772	1.44
	94/07/23	$1.88^{+0.01}_{-0.01}$	$0.67^{+0.01}_{-0.01}$	$0.12^{+0.01}_{-0.01}$	$0.011^{+0.002}_{-0.002}$	2861.5/1013	2.82
	97/08/03	$1.80^{+0.01}_{-0.01}$	$0.91^{+0.03}_{-0.03}$	$0.07^{+0.03}_{-0.03}$	$0.032^{+0.004}_{-0.004}$	1972.6/1013	1.95
	97/08/07	$1.77^{+0.01}_{-0.01}$	$0.73^{+0.03}_{-0.03}$	$0.15^{+0.03}_{-0.03}$	$0.036^{+0.003}_{-0.004}$	1649.4/1015	1.63
MR 2251-178	94/04/02	$1.81^{+0.02}_{-0.02}$	$0.40^{+0.07}_{-0.07}$	$0.17^{+0.05}_{-0.06}$	$0.000^{+0.003}_{-0.000}$	829.3/823	1.01
	93/12/07	$1.75^{+0.02}_{-0.02}$	$0.41^{+0.06}_{-0.05}$	$0.10^{+0.04}_{-0.04}$	$0.000^{+0.004}_{-0.000}$	821.7/867	0.95
	93/12/14	$1.67^{+0.03}_{-0.02}$	$0.40^{+0.08}_{-0.09}$	$0.09^{+0.07}_{-0.05}$	$0.000^{+0.007}_{-0.000}$	768.0/750	1.02
	93/12/19	$1.63^{+0.04}_{-0.04}$	$0.5^{+0.1}_{-0.1}$	$0.065^{+0.08}_{-0.07}$	$0.01^{+0.02}_{-0.00}$	628.1/696	0.90
	93/12/24	$1.57^{+0.03}_{-0.03}$	$0.41^{+0.08}_{-0.09}$	$0.00^{+0.06}_{-0.00}$	$0.000^{+0.004}_{-0.000}$	634.4/660	0.96
NGC3516	94/04/02	$1.71^{+0.01}_{-0.01}$	$0.74^{+0.03}_{-0.03}$	$0.39^{+0.02}_{-0.03}$	$0.0^{+0.0}_{-0.0}$	924.3/772	1.20
	95/03/11	$1.72^{+0.03}_{-0.02}$	$0.64^{+0.05}_{-0.05}$	$0.21^{+0.05}_{-0.03}$	$0.05^{+0.01}_{-0.01}$	1025.6/1005	1.02
	95/03/12	$1.78^{+0.01}_{-0.02}$	$0.64^{+0.04}_{-0.04}$	$0.16^{+0.04}_{-0.04}$	$0.028^{+0.005}_{-0.007}$	1079.1/1002	1.08
NGC4051	93/07/27	$2.37^{+0.01}_{-0.01}$	$0.01^{+0.03}_{-0.01}$	$0.55^{+0.03}_{-0.03}$	$0.0^{+0.0}_{-0.0}$	1320.4/748	1.77
	96/06/27	$2.219^{+0.010}_{-0.004}$	$0.00^{+0.01}_{-0.00}$	$0.25^{+0.01}_{-0.01}$	$0.0^{+0.0}_{-0.0}$	1746.6/1010	1.73
NGC5548	93/07/27	$1.92^{+0.01}_{-0.01}$	$0.28^{+0.03}_{-0.03}$	$0.14^{+0.03}_{-0.03}$	$0.0^{+0.0}_{-0.0}$	829.8/772	1.07
	96/06/27	$1.91^{+0.02}_{-0.02}$	$0.3631^{+0.04}_{-0.04}$	$0.08^{+0.03}_{-0.03}$	$0.047^{+0.005}_{-0.005}$	1156.1/1011	1.14
	96/06/29	$1.89^{+0.02}_{-0.01}$	$0.65^{+0.04}_{-0.04}$	$0.000^{+0.009}_{-0.000}$	$0.031^{+0.006}_{-0.005}$	1249.5/999	1.25
	96/07/01	$1.84^{+0.02}_{-0.02}$	$0.69^{+0.05}_{-0.06}$	$0.016^{+0.04}_{-0.02}$	$0.041^{+0.007}_{-0.007}$	1096.4/1002	1.09
	96/07/03	$1.75^{+0.03}_{-0.02}$	$0.56^{+0.04}_{-0.06}$	$0.01^{+0.05}_{-0.01}$	$0.03^{+0.01}_{-0.01}$	995.5/984	1.01
	96/07/04	$1.77^{+0.02}_{-0.01}$	$0.56^{+0.02}_{-0.05}$	$0.00^{+0.04}_{-0.00}$	$0.03^{+0.01}_{-0.00}$	1105.1/1008	1.10
	98/06/15	$1.94^{+0.01}_{-0.01}$	$0.28^{+0.02}_{-0.03}$	$0.00^{+0.02}_{-0.00}$	$0.046^{+0.004}_{-0.004}$	988.4/774	1.28
	98/06/20	$1.944^{+0.004}_{-0.004}$	$0.281^{+0.009}_{-0.015}$	$0.000^{+0.006}_{-0.000}$	$0.051^{+0.001}_{-0.001}$	2115.6/774	2.73
	98/07/07	$1.78^{+0.02}_{-0.01}$	$0.16^{+0.03}_{-0.05}$	$0.01^{+0.04}_{-0.01}$	$0.03^{+0.01}_{-0.01}$	1006.4/902	1.12
	99/01/19	$1.84^{+0.03}_{-0.03}$	$0.24^{+0.07}_{-0.06}$	$0.03^{+0.05}_{-0.03}$	$0.06^{+0.01}_{-0.01}$	697.0/664	1.05

Table 2. Spectral fitting absorption results for the phenomenological model, as defined in Section 3.2 of the main text. Column 3 shows the best fitting power law photon index. Column 4 and 5 give the optical depths at threshold of the OVII and OVIII absorption edges respectively. Column 6 reports the best fitting column density of intrinsic neutral absorbing material (placed at the redshift of the source). Column 7 gives the goodness of the fit parameter and the number of degrees of freedom (dof). Finally, column 8 presents the Red. χ^2 of the fit.

photoionization code Cloudy C90.04 (Ferland et al. 1998). Initially, a power-law ionizing continuum has been used, of photon index Γ (determined by the phenomenological model above), and luminosity between 2–10 keV, L_{2-10} equal to 10^{43} erg s^{-1}, incident onto a shell at inner radius $r = 10^{16}$ cm of density $n = 5 \times 10^9$–10^{13} cm^{-3}. Therefore, the ionization parameter:

$$\xi = \frac{L_{2-10}}{nr^2} \qquad (4)$$

varies from 0.01 to 20 erg cm s^{-1}. The column density was varied from $N_{\rm wa} = 10^{20.3}$–10^{24} cm^{-2}. NGC 4051 is the only object in our sample that has $\Gamma > 2$ and also the only source presenting absorption features at energies larger than 1 keV. It required larger values for the ionization parameter: 1–50 erg cm s^{-1}; hence the range of values covered by the density is $n = 5 \times 10^{10}$–10^{11} cm^{-3}. We will be assuming a constant density cloud in our modelling, which may not be true in every case (e.g. Binette 1998). A black body has been included for MCG−6-30-15, NGC 3516, NGC 4051, and NGC 5548 as given in Table 3. Recall that spectral variability of MCG−6-30-15 strongly argues for a multi-zone warm absorber (e.g. Otani et al. 1996, Morales, Fabian and Reynolds 2000, Lee et al. 2001). The simultaneous UV/X-ray studies of NGC3516 by Kriss et al. (1996a,b) also imply the existence of a complex stratified ionized absorber. The *Chandra* observation of NGC 4051 (Collinge et al. 2001) has revealed a two-zone WA for this object. Thus, one-zone photoionization models can be only regarded as a useful parameterization of the spectral data.

All the observations for each source were examined using Cloudy models of the type described above. The results of these fits are shown in Table 4. The data still show devi-

Date of Observation	Photon index Γ	kT (keV)	τ_{O7}	τ_{O8}	Intrinsic $N_{\rm H}$ (10^{22} cm^{-2})	χ^2/dof	Red. χ^2	$L_{\rm B}$ (10^{43} erg s^{-1})	$L_{\rm B}/L_{2-10}$
MCG−6-30-15									
1993/07/09	$1.96^{+0.02}_{-0.02}$	$0.09^{+0.01}_{-0.01}$	$0.61^{+0.05}_{-0.04}$	$0.10^{+0.03}_{-0.03}$	$0.03^{+0.03}_{-0.02}$	797.5/767	1.04	0.6	0.46
1993/07/31	$1.83^{+0.02}_{-0.04}$	$0.11^{+0.01}_{-0.01}$	$0.8^{+0.1}_{-0.1}$	$0.19^{+0.04}_{-0.05}$	$0.11^{+0.03}_{-0.05}$	785.8/764	1.03	1.1	1.09
1994/07/23	$1.91^{+0.01}_{-0.01}$	$0.10^{+0.01}_{-0.00}$	$0.65^{+0.03}_{-0.01}$	$0.11^{+0.01}_{-0.01}$	$0.05^{+0.02}_{-0.01}$	1286.3/1005	1.28	0.3	0.24
1997/08/03	$1.85^{+0.01}_{-0.01}$	$0.080^{+0.004}_{-0.004}$	$0.78^{+0.02}_{-0.02}$	$0.04^{+0.01}_{-0.01}$	$0.11^{+0.01}_{-0.01}$	1208.7/1005	1.20	1.2	1.08
1997/08/07	$1.81^{+0.01}_{-0.02}$	$0.10^{+0.02}_{-0.01}$	$0.70^{+0.04}_{-0.04}$	$0.13^{+0.03}_{-0.03}$	$0.10^{+0.01}_{-0.03}$	1004.6/1007	1.00	0.5	0.46
NGC3516									
1994/04/02	$1.68^{+0.01}_{-0.01}$	$0.10^{+0.01}_{-0.01}$	$0.74^{+0.04}_{-0.04}$	$0.31^{+0.03}_{-0.03}$	$0.02^{+0.02}_{-0.02}$	886.8/767	1.16	0.3	0.1
1995/03/11	$1.73^{+0.03}_{-0.03}$	$0.14^{+0.03}_{-0.01}$	$0.66^{+0.05}_{-0.05}$	$0.25^{+0.04}_{-0.04}$	$0.05^{+0.02}_{-0.01}$	1001.2/1000	1.0	0.04	0.02
1995/03/12	$1.81^{+0.02}_{-0.03}$	$0.08^{+0.01}_{-0.02}$	$0.57^{+0.04}_{-0.07}$	$0.16^{+0.05}_{-0.04}$	$0.06^{+0.02}_{-0.02}$	1043.1/997	1.04	0.6	0.4
NGC4051									
1993/04/25	$2.06^{+0.03}_{-0.02}$	$0.11^{+0.00}_{-0.01}$	$0.23^{+0.05}_{-0.09}$	$0.15^{+0.04}_{-0.06}$	$0.00^{+0.03}_{-0.00}$	883.6/743	1.19	0.6	27.1
1994/06/07	$2.01^{+0.02}_{-0.01}$	$0.13^{+0.01}_{-0.01}$	$0.22^{+0.04}_{-0.03}$	$0.12^{+0.02}_{-0.02}$	$0.02^{+0.03}_{-0.01}$	1145.4/1005	1.14	0.5	15.0
NGC5548									
1993/07/27	$1.86^{+0.02}_{-0.02}$	$0.16^{+0.01}_{-0.02}$	$0.37^{+0.03}_{-0.04}$	$0.15^{+0.03}_{-0.03}$	$0.00^{+0.01}_{-0.00}$	780.0/767	1.01	0.4	0.1
1996/06/27	$1.91^{+0.02}_{-0.02}$	$0.14^{+0.01}_{-0.02}$	$0.38^{+0.04}_{-0.04}$	$0.15^{+0.03}_{-0.03}$	$0.06^{+0.01}_{-0.01}$	1075.2/1006	1.07	0.5	0.1
1996/06/29	$1.85^{+0.03}_{-0.03}$	$0.16^{+0.02}_{-0.03}$	$0.73^{+0.04}_{-0.05}$	$0.00^{+0.04}_{-0.00}$	$0.03^{+0.01}_{-0.01}$	1164.9/994	1.17	0.5	0.1
1996/07/01	$1.82^{+0.04}_{-0.03}$	$0.16^{+0.02}_{-0.02}$	$0.70^{+0.06}_{-0.06}$	$0.10^{+0.05}_{-0.04}$	$0.05^{+0.01}_{-0.01}$	1028.2/997	1.03	0.4	0.1
1996/07/03	$1.80^{+0.02}_{-0.02}$	$0.06^{+0.01}_{-0.00}$	$0.3^{+0.1}_{-0.1}$	$0.00^{+0.03}_{-0.00}$	$0.12^{+0.03}_{-0.02}$	915.7/979	0.94	25.9	5.1
1996/07/04	$1.78^{+0.03}_{-0.02}$	$0.14^{+0.02}_{-0.02}$	$0.6^{+0.1}_{-0.1}$	$0.07^{+0.04}_{-0.04}$	$0.05^{+0.01}_{-0.01}$	1021.1/1003	1.02	0.8	0.1
1998/06/15	$1.96^{+0.02}_{-0.02}$	$0.11^{+0.01}_{-0.01}$	$0.32^{+0.03}_{-0.03}$	$0.04^{+0.03}_{-0.03}$	$0.07^{+0.02}_{-0.01}$	828.8/769	1.10	1.7	0.2
1998/06/20	$1.96^{+0.01}_{-0.01}$	$0.132^{+0.003}_{-0.004}$	$0.34^{+0.01}_{-0.02}$	$0.07^{+0.02}_{-0.01}$	$0.08^{+0.00}_{-0.01}$	1028.7/769	1.34	1.8	0.2
1998/07/07	$1.84^{+0.03}_{-0.02}$	$0.15^{+0.01}_{-0.01}$	$0.23^{+0.06}_{-0.05}$	$0.12^{+0.05}_{-0.04}$	$0.07^{+0.02}_{-0.01}$	772.8/740	1.04	0.9	0.2
1999/01/19	$1.81^{+0.03}_{-0.06}$	$0.19^{+0.05}_{-0.03}$	$0.25^{+0.08}_{-0.05}$	$0.10^{+0.06}_{-0.06}$	$0.07^{+0.01}_{-0.01}$	674.6/659	1.02	0.4	0.1

Table 3. Spectral fitting results for the phenomenological model including a black body component for MCG−6-30-15, NGC 3516, NGC 4051 and NGC 5548. Column 2 gives the best fitting power law photon index. Column 3 presents the best fitting black body temperature. Column 4 and 5 give the optical depths at threshold of the OVII and OVIII absorption edges respectively. Column 6 reports the best fitting column density of intrinsic neutral absorbing material (placed at the redshift of the source). Column 7 gives the goodness of the fit parameter and the number of degrees of freedom (dof). Column 8 presents the Red. χ^2 of the fit. Column 9 reports the total (bolometric) luminosity of the best fitting black body and Column 10 shows the ratio of this bolometric luminosity to the 2–10 keV luminosity.

ations from this best fitting at ~ 1 keV. This presumably signals a breakdown in one of the assumptions of this model (such as the one-zone nature or the chemical abundances of the plasma).

An illustration of the incident and transmitted continuum as calculated by our models and the confidence contour plot for two observations of MCG−6-30-15 and NGC 5548 is illustrated in Fig. 1[†]. In Table 5 the values for $L_{\rm abs}$ for each of the 30 observations is reported.

3.3 Results and comparison with other estimates

3.3.1 Mean values, errors and comparison with other methods

We have substituted the results of $L_{\rm abs}$ and $N_{\rm wa}$ from each observation in Eqn. 2. The value of the black hole mass, $M_{\rm BH}$ for each observation versus the 2–10 keV luminosity, L_{2-10} is presented in Fig. 2 and reported in Table 6. There are differences in the results for $M_{\rm BH}$ obtained for each observation that can be accounted for within the errors, except for one observation of NGC 3516[‡]. A possible cause for these differences could be the dynamical evolution of the WA, since we would be proving different material for different observations. In particular for the case of the NGC 3516 UV and

[†] The incident and transmitted continuum as calculated by our models for all the observations as well as all the contour plots are presented at `http://www-xray.ast.cam.ac.uk/~rm/BH_mass/`

[‡] See Table 4. The 2–10 luminosity for this source in the 1994 observation is approximately 2 times larger than in those observations in 1995. Also note how our photoionization model does not reproduce very well this very first observation, giving a $\chi^2 = 1.91$.

Source	Date of Observation	$\log N_{\rm wa}$ cm^{-2}	ξ (erg cm^{-2} s^{-1})	Intrinsic $N_{\rm H}$ (10^{22} cm^{-2})	L_{2-10} (10^{43} erg s^{-1})	χ^2/dof	Red. χ^2
IC4329a	1993/08/15	$21.49^{+0.04}_{-0.04}$	$1.4^{+0.5}_{-0.4}$	$0.24^{+0.01}_{-0.01}$	7.4	1091.3/773	1.41
	1997/08/07	$21.1^{+0.1}_{-0.1}$	$1.0^{+0.9}_{-0.3}$	$0.39^{+0.0}_{-0.2}$	10.1	1314.6/1008	1.30
	1997/08/10	$21.3^{+0.1}_{-0.1}$	$1.6^{+0.4}_{-0.8}$	$0.31^{+0.02}_{-0.01}$	7.5	824.6/775	1.07
	1997/08/12	$21.2^{+0.1}_{-0.1}$	$4.^{+3.}_{-3.}$	$0.42^{+0.02}_{-0.02}$	8.6	899.2/773	1.16
	1997/08/15	$21.79^{+0.02}_{-0.03}$	$0.3^{+0.5}_{-08.}$	$0.03^{+0.03}_{-0.02}$	10.4	1283.5/1006	1.28
MCG−6-30-15	1993/07/09	$21.77^{+0.02}_{-0.02}$	$8.2^{+0.3}_{-0.3}$	$0.^{+0.}_{-0.}$	1.3	1159.3/773	1.50
	1993/07/31	$21.96^{+0.03}_{-0.04}$	$12.^{+1.}_{-1.}$	$0.^{+0.}_{-0.}$	1.1	1115.5/770	1.45
	1994/07/23	$21.62^{+0.04}_{-0.01}$	$4.4^{+0.6}_{-0.6}$	$0.^{+0.}_{-0.}$	1.2	1.933.2/1011	1.91
	1997/08/03	$21.70^{+0.08}_{-0.02}$	$4.2^{+0.1}_{-0.1}$	$0.^{+0.}_{-0.}$	1.0	1568.5/1010	1.55
	1997/08/07	$21.67^{+0.01}_{-0.01}$	$4.1^{+0.1}_{-0.1}$	$0.^{+0.}_{-0.}$	0.9	1312.3/1013	1.30
MR 2251-178	1993/11/16	$21.6^{+0.1}_{-0.1}$	$9.^{+2.}_{-1.}$	$0.^{+0.}_{-0.}$	81.4	771.5/759	1.02
	1993/12/07	$21.5^{+0.1}_{-0.1}$	$8.^{+1.}_{-1.}$	$0.^{+0.}_{-0.}$	91.4	840.3/868	0.97
	1993/12/14	$21.5^{+0.1}_{-0.1}$	$8.^{+2.}_{-2.}$	$0.^{+0.}_{-0.}$	80.8	776.0/751	1.03
	1993/12/19	$21.5^{+0.1}_{-0.1}$	$7.^{+1.}_{-2.}$	$0.^{+0.}_{-0.}$	77.3	635./697	0.91
	1993/12/24	$21.4^{+0.1}_{-0.1}$	$9.^{+4.}_{-1.}$	$0.^{+0.}_{-0.}$	62.5	640.3/661	0.97
NGC3516	1994/04/02	$21.80^{+0.01}_{-0.01}$	$9.3^{+0.1}_{-0.0}$	$0.^{+0.}_{-0.}$	2.5	1475.2/773	1.91
	1995/03/11	$21.63^{+0.02}_{-0.02}$	$3.6^{+0.4}_{-0.3}$	$0.^{+0.}_{-0.}$	1.6	1105.2/1006	1.10
	1995/03/12	$21.64^{+0.02}_{-0.02}$	$4.2^{+0.4}_{-0.3}$	$0.^{+0.}_{-0.}$	1.5	1151.4/1003	1.15
NGC4051	1993/04/25	$22.45^{+0.03}_{-0.04}$	$41.^{+2.}_{-3.}$	$0.^{+0.}_{-0.}$	0.03	1585.1/749	2.11
	1994/06/07	$22.43^{+0.01}_{-0.02}$	$48.^{+1.}_{-1.}$	$0.^{+0.}_{-0.}$	0.04	1982.0/1011	1.96
NGC5548	1993/07/27	$21.5^{+0.1}_{-0.0}$	$11.^{+3.}_{-1.}$	$0.^{+0.}_{-0.}$	4.9	899.5/773	1.16
	1996/06/27	$21.41^{+0.01}_{-0.03}$	$3.3^{+0.5}_{-0.7}$	$0.03^{+0.00}_{-0.00}$	7.6	1196.1/1012	1.18
	1996/06/29	$21.40^{+0.02}_{-0.02}$	$1.6^{+0.2}_{-0.2}$	$0.^{+0.}_{-0.}$	6.8	1288.8/1000	1.29
	1996/07/01	$21.45^{+0.01}_{-0.02}$	$1.6^{+0.2}_{-0.1}$	$0.^{+0.}_{-0.}$	5.6	1140.6/1003	1.14
	1996/07/03	$21.45^{+0.02}_{-0.02}$	$1.8^{+0.4}_{-0.3}$	$0.^{+0.}_{-0.}$	4.8	999.5/985	1.01
	1996/07/04	$21.40^{+0.01}_{-0.03}$	$1.8^{+0.2}_{-0.3}$	$0.^{+0.}_{-0.}$	5.9	1130.8/1009	1.12
	1998/06/15	$21.19^{+0.03}_{-0.02}$	$2.0^{+1.0}_{-0.2}$	$0.04^{+0.00}_{-0.00}$	7.0	1018.8/775	1.31
	1998/06/20	$21.16^{+0.03}_{-0.06}$	$1.1^{+0.4}_{-0.6}$	$0.03^{+0.00}_{-0.00}$	8.2	2447.0/775	2.90
	1998/07/07	$21.15^{+0.02}_{-0.06}$	$0.4^{+0.3}_{-0.1}$	$0.^{+0.}_{-0.}$	5.1	849.1/746	1.14
	1999/01/19	$21.15^{+0.07}_{-0.05}$	$4.^{+2.}_{-1.}$	$0.05^{+0.01}_{-0.01}$	5.5	702.8/665	1.06

Table 4. Spectral fitting results using the one-zone photoionization model. Columns 3 and 4 give the best-fitting column density and ionization parameter ξ of the warm photoionized plasma. Column 5 gives the best fitting column density of intrinsic neutral absorbing material (placed at the redshift of the source). Column 6 reports the goodness of the fit parameter and column 7 the Red. χ^2 of the fit.

X-ray absorber, such evolution has been reported (Koratkar et al. 1996 and Kriss et al. 1996b).

It is worth noting that all the MR2251-178 observations were taken within one month and for this particular object the consistency of the results is remarkable. There is also a variation in L_{2-10} with time for all the sources (i.e. the source gets brighter or fainter). These changes in the X-ray luminosity do not seem to relate to the values obtained for $M_{\rm BH}$ in a simple manner.

For several of these AGN, there is extensive observational evidence for a multi-zone WA. For the case of MCG−6-30-15, time variability of the OVIII edge (e.g. Otani et al. 1996, Morales et al. 2000) and the detection of different ionization species (Lee et al. 2001) support the multi-zone hypothesis. And very recently, for the case of NGC 4051, Collinge et al. (2001) have resolved two distinct absorption systems. We have not taken into account the multi-zone nature of the WA in the present work.

Another element that might have some effect on our results is that below approximately 1 keV SIS0 and SIS1 spectra since approximately late 1994 have been showing an increasing divergence from each other, and from the GIS data, towards lower energies. This is in the sense that both SIS0 and SIS1 efficiencies below 1 keV have been steadily decreasing over time. This loss in efficiency is currently not corrected by any of the software and a detailed analysis of how this could affect our results is discussed in Section 3.3.2.

Once the value of the black hole mass was calculated for each observation, we have obtained the mean value for each source. For that, those observations with $\chi^2 > 2$ have been excluded. Our result for NGC 4051 might not be significant giving the high value of χ^2 for both observations

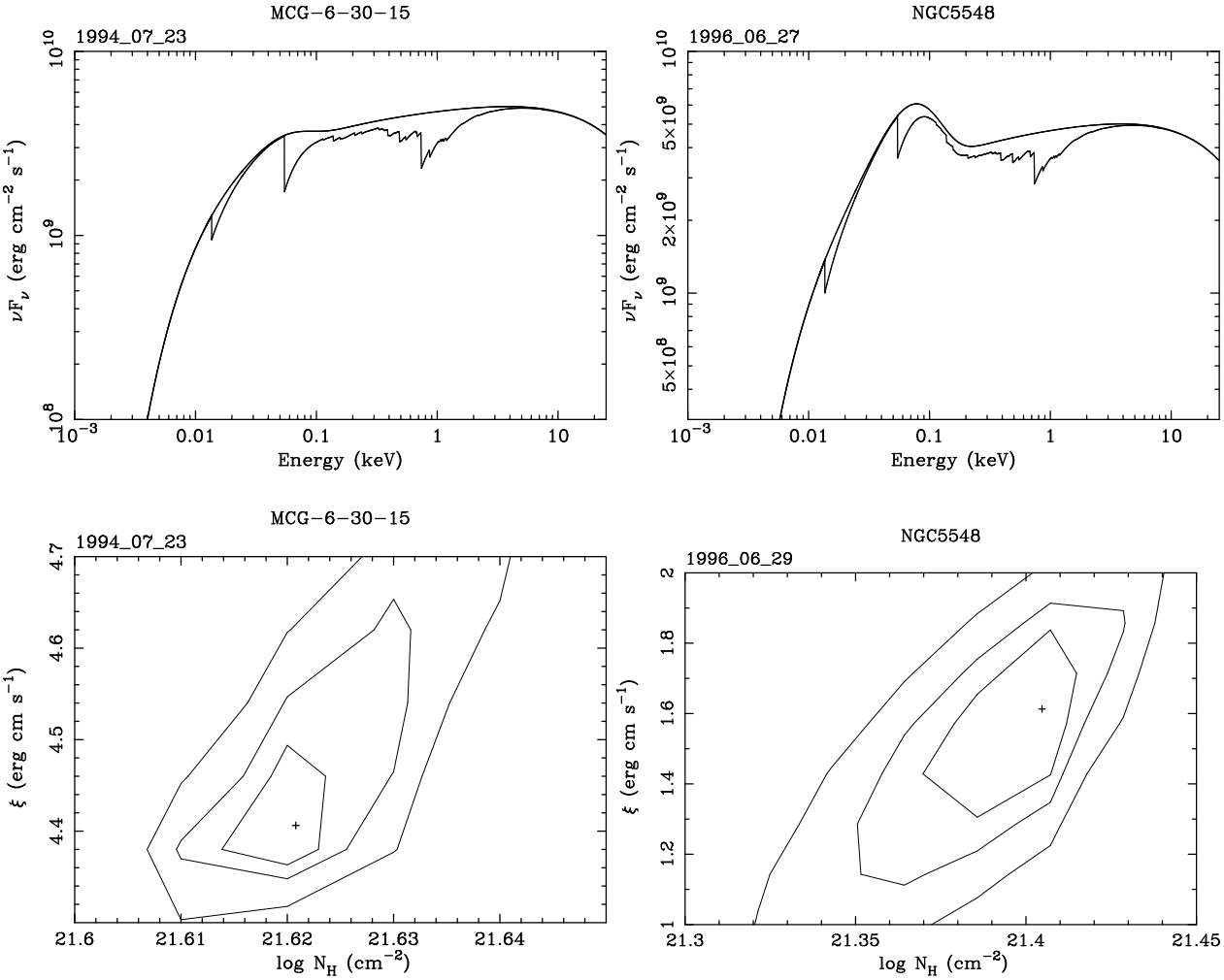

Figure 1. Top panels: example of the incident continuum (top line) and transmitted continuum (bottom line) as predicted by our models for the 1994/07/23 MCG−6-30-15 and the 1996/06/27 NGC 5548 observations. The area enclosed by the two lines gives the value for the flux absorbed by the WA clouds. Bottom panels: contour plots for the two observations in the plane ionization parameter, ξ, against column density, $N_{\rm wa}$ at the 68, 90 and 99 per cent confident level for the two parameters of interest.

(although our result is consistent with other methods estimates). The errors only take into account the uncertainties in $L_{\rm abs}$ (calculated from the dispersion in the value of $L_{\rm abs}$ for each observation) and $N_{\rm wa}$ (obtained from the fits). The mean values for $M_{\rm BH}$ are presented in Figure 3 together with other independent methods estimates: reverberation mapping (Wandel et al. 1999) for IC4329a, NGC 4051, and NGC 5548; X-ray variability (Czerny et al. 2000) for MCG−6-30-15, NGC 4051, and NGC 5548; and velocity dispersion results (Gebhardt et al. 2000) for NGC 3516 and NGC 4051. Our estimates for all sources cluster around 10^7 $M_\odot$. Despite the simplicity of our model, our results reproduce within an order of magnitude other independent estimates.

3.3.2 The case of NGC4051

At low energies, the X-ray continuum of NGC 4051 has been observed to be dominated by a variable soft excess (e.g. Turner & Pounds 1989; Guainazzi et al. 1996). Guainazzi et al. (1996) also argued for significant variability of the OVII edge while the OVIII edge remained roughly constant in strength, precisely the reverse of the behavior seen in MCG−6-30-15 (Reynolds 1997). This object has very recently been observed with *Chandra* (Collinge et al. 2001), and they clearly detect a two-zone WA.

There are only two observations for NGC 4051 and both of them, when fitted to our photoionization models, give a $\chi^2 \sim 2$. This indicates that our model breaks down for this particular object. In Section 3.2 it was already noted that NGC 4051 was the only object in our sample that has $\Gamma > 2$ and also the only source presenting absorption features at energies larger than 1 keV .

We have investigated if the reason for this disagreement could be the divergence between SIS0 and SIS1 spectra and from the GIS data, since approximately late 1994. To test this hypothesis we have analysed each detector individually. Table 7 reports the results and Fig. 4 gives a graphical representation of them. Surprisingly the only result that is inconsistent with the rest is one given by GIS2 in the first observation. Apart from this single value, the other estimates are consistent with those obtained for the case of the full

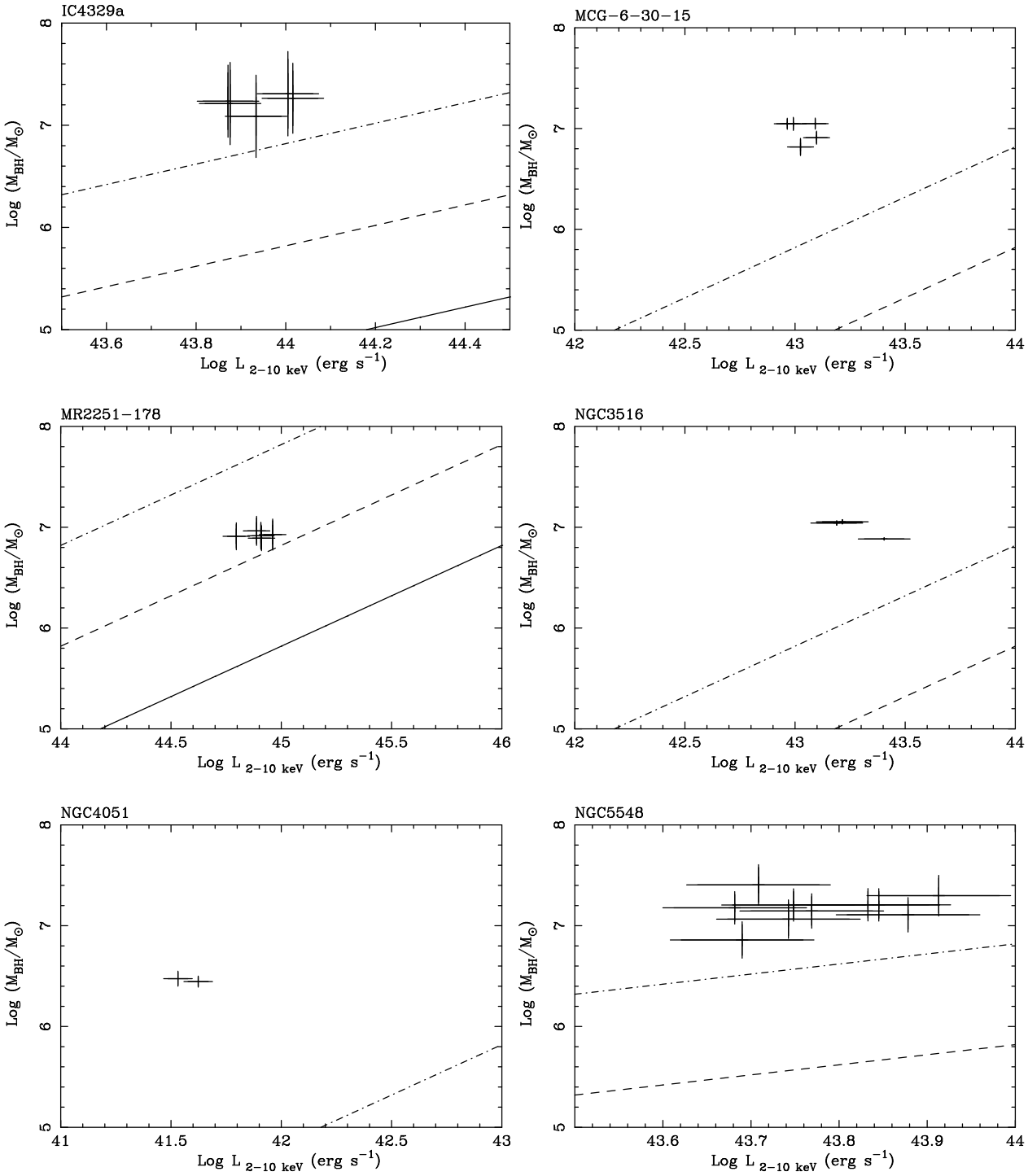

Figure 2. Black hole mass, $M_{\rm BH}$, in solar units for the 30 observations of the 6 AGN (the names of the objects appear at the top left corner of each figure) versus the 2–10 keV luminosity, L_{2-10}. The solid line corresponds to $L = L_{\rm Edd}$, the dashed line to $L = 0.1L_{\rm Edd}$, and the dot-dashed line to $L = 0.01L_{\rm Edd}$, where $L = 10L_{2-10}$.

analysis, favoring the singular nature of NGC 4051 as the cause for not fitting a single ionization parameter model.

4 THE INFLUENCE OF THE UNDERLYING CONTINUUM ON OUR ESTIMATE

The emitted spectrum of Type 1 galaxies in the extreme UV/very soft X-ray band is poorly known although the photons are highly effective at ionizing warm absorbing gas. Study of the effect of the excess soft X-ray emission on our results is therefore of great importance. The object we have

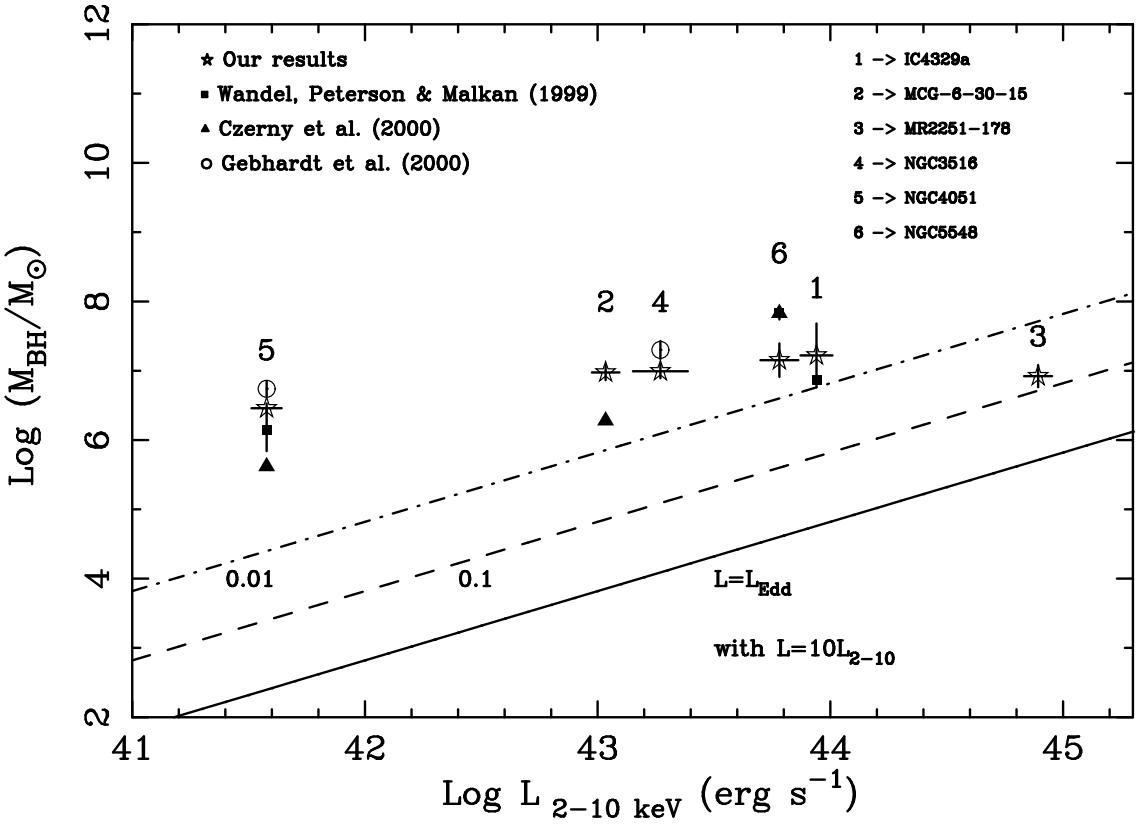

Figure 3. Our results for the mean black hole mass (stars) of the six sources versus the mean 2 to 10 keV luminosity, L_{2-10}. Other estimates (reverberation mapping (Wandel, Peterson & Malkan 1999), marked as squares for IC4329a, NGC 4051, and NGC 5548, X-ray variability (Czerny et al. 1999) , marked as triangles for MCG−6-30-15, NGC 4051, and NGC 5548, and velocity dispersion (Gebhardt et al. 2000), marked as circles for NGC 3516 and NGC 4051) have been plotted at our mean L_{2-10}. Reminder: **our results are upper limits on the black hole mass** and are not marked as such to avoid confusion. The solid line corresponds to $L = L_{\rm Edd}$, the dashed line to $L = 0.1L_{\rm Edd}$, and the dot-dashed line to $L = 0.01L_{\rm Edd}$, where $L = 10L_{2-10}$.

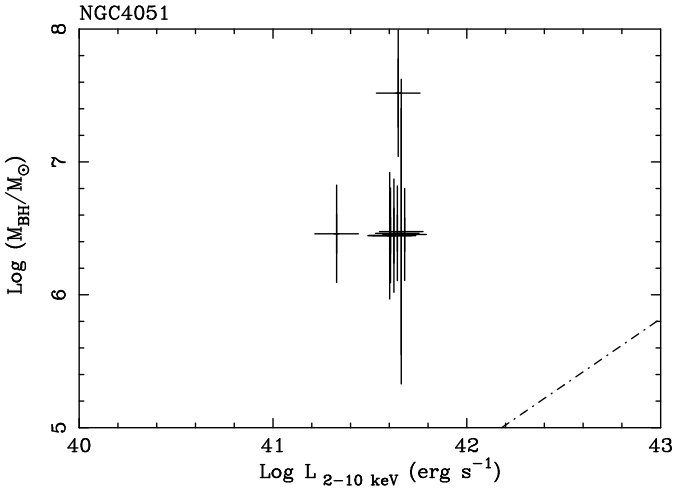

Figure 4. Values obtained for the BH mass of NGC 4051 when the 4 different *ASCA* instrument are independently fitted for the 1993 and 1994 observations of our sample. The dot-dashed line corresponds to $L = 0.01L_{\rm Edd}$, where $L = 10L_{2-10}$.

selected to study the influence of a different underlying continuum has been NGC 5548. The reason for that has been the availability of a model for its intrinsic spectrum (i.e. after the effect of Galactic absorption at the soft excess and reddening at the optical/UV spectrum has been removed), as given by Magdziarz et al. (1998). Also for this particular object there are 10 different observation in our sample, which allow us a better comparison with our results.

Fig. 5, left panel, presents a montage of the incident and transmitted continuum as calculated by our photoionization models for 4 observations of this object. The different soft excess for each observation generated a different level of ionization in the WA and therefore the spectrum for different observations present different absorption edges (e.g. for observation 1998/07/07, labeled 9 in Fig. 5, the absorption edges for $\rm H_I$ and $\rm He_{II}$ at at 0.0136 keV and 0.0544 keV, respectively, are very prominent). However, since the soft X-ray spectrum has to be reproduced by the models after the ionizing radiation has passed through the WA, the black hole mass estimate through the ratio $L_{\rm abs}/N_{\rm wa}$ would regulate itself to changes in either quantity (i.e. higher values for the luminosity absorbed demand higher values for the column density and a strong EUV excess means that He is more highly ionized). As seen in Table 6, the errors can account for the differences in the results.

The comparison between the BH mass estimates obtained using our underlying continuum, $(M_{\rm BH}/M_\odot)_{\rm cont.a}$, and those using the Magdziarz et al. (1998) spectrum,

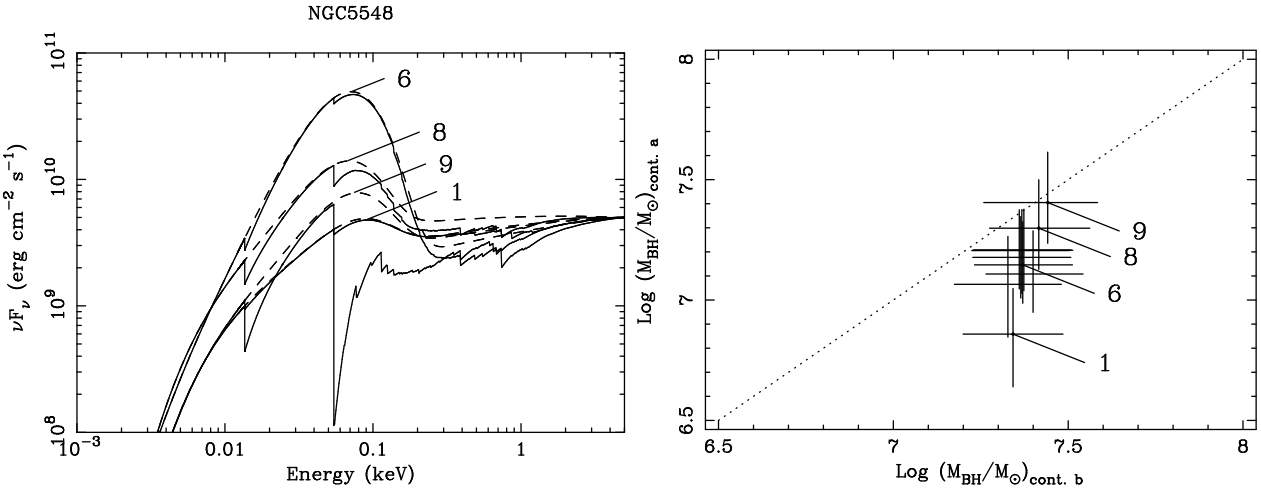

Figure 5. Left panel: Incident (dashed line) and transmitted (solid line) continuum for the 1 (1993/07/27), 6 (1996/07/04), 8 (1998/06/20), and 9 (1998/07/07) observations of NGC 5548, as calculated by our photoionization models. This figure shows the differences in the incident continuum for these observations, as well as graphically presenting the different amounts of luminosity absorbed by the WA. The absorption edges for H_I and He_{II} at at 0.0136 keV and 0.0544 keV , respectively, become very prominent for some observations. Right panel: Comparison of the results for the BH masses using our underlying continuum, $(M_{BH}/M_\odot)_{cont.a}$, versus those obtained using Magdziarz et al. (1998) continuum, $(M_{BH}/M_\odot)_{cont.b}$. The dotted line marks the equality of both values. The 1 (1993/07/27), 6 (1996/07/04), 8 (1998/06/20), and 9 (1998/07/07) observations are labeled.

$(M_{BH}/M_\odot)_{cont.b}$, is illustrated in Fig. 5, right panel. The former results appear to be lower than the latter, but still the differences are accounted for within the errors.

5 ANALYSIS OF FURTHER TERMS IN THE EQUATION OF MOTION

5.1 The drag term

This section discusses the possibility of a drag force acting on the WA clouds, and also presents some problems that the cloud model raises. For the purposes of estimating the black hole mass, the gas that is responsible for the WA is assumed to exist as isolated clouds which are likely moving through an intercloud (IC) medium. These clouds could be confined by a hot IC medium. A two-phase model, i.e. cold clouds embedded in a hot IC medium, for the broad and narrow line regions in quasars, BLR and NLR, respectively, has been extensively studied (e.g. Krolik et al. 1981, Mathews & Murray 1987). The major objection to the model is the cloud confinement problem (if the clouds are not continuously formed, an external mechanism is necessary). Another problem is cloud break-up by drag forces. The difficulties with the model, especially in relation to the hot medium temperature, are discussed in Fabian et al. (1986) and Mathews & Ferland (1987). The latter reference discusses the dynamical implications of the two-phase model. Also in Elitzur & Ferland (1986) the stability of these clouds is addressed. Our WA cloud model will be subject to all these caveats. The IC medium could have a very significant effect on the dynamics of the clouds through its drag and the resulting hydrodynamic instabilities. Whether the WA clouds can move relative to a IC medium without suffering gravitational, tidal, shear, or Rayleigh-Taylor instabilities is beyond the scope of this work. We assume that magnetic fields internal to the clouds must be important.

First we note that ignoring the drag force justifies hving chosen our estimates as upper limits. If the density of this external gas is large enough then the WA would be subject to a drag force that would cause us to overestimate the strength of gravity in the dynamics of the WA. The upper-limit of the black hole mass is found by assuming that the radiation force on the WA, F_{rad}, is larger than the gravitational restoring force, F_{grav}. Therefore, the drag force will be important if it is comparable to F_{rad}:

$$\frac{AL_{abs}}{4\pi r^2 c} \approx \rho_0 v^2 A. \quad (5)$$

The density of the IC medium at which drag will be important can then be related to the velocity of the WA through the medium (which we take to be the observed radial velocity):

$$n_0 = \frac{L_{abs}}{4\pi r^2 c \mu v^2}, \quad (6)$$

where μ is the mean mass of particles in the intercloud medium (assumed to be a pure hydrogen and helium mixture). Making use of the average L_{abs} for each object, we plot in Figure 6 this critical density as a function of the outflowing velocity of the WA. A distance of $r = 10^{16}$ cm was assumed, and the range in v was chosen to cover the range that is typically observed in WAs. If the density of the IC medium is below the line then drag is not important; alternatively, drag will be important if the IC density lies above the line. For typical values of the observed WA blueshift, an IC density $\gtrsim 10^7$ cm^{-3} seems to be required for drag to be important in any of the objects. The most direct limits of the gas come from opacity arguments (i.e. the absence of soft X-ray absorption). We shall note at this stage that a medium with a density of 10^7 cm^{-3} and a pathlength of 10^{16} cm has a Thomson depth of nearly 0.1.

Another constraint on the properties of the IC medium is that its column density has to be smaller than that of the

Source	Date of Observation	$\log L_{\rm abs}$ (erg s $^{-1}$)
IC4329a	93/08/15	42.6 ± 0.3
	97/08/07	42.3 ± 0.3
	97/08/10	42.4 ± 0.3
	97/08/12	42.2 ± 0.3
	97/08/15	43.0 ± 0.3
MCG−6-30-15	93/07/09	42.60 ± 0.05
	93/07/31	42.70 ± 0.05
	94/07/23	42.59 ± 0.05
	97/08/03	42.67 ± 0.05
	97/08/07	42.64 ± 0.05
MR 2251-178	94/04/02	42.42 ± 0.06
	93/12/07	42.37 ± 0.06
	93/12/14	42.33 ± 0.06
	93/12/19	42.37 ± 0.06
	93/12/24	42.24 ± 0.06
NGC3516	94/04/02	42.608 ± 0.001
	95/03/11	42.609 ± 0.001
	95/03/12	42.606 ± 0.001
NGC4051	93/04/25*	42.85 ± 0.05
	94/06/07	42.80 ± 0.05
NGC5548	93/07/27	42.3 ± 0.2
	96/06/27	42.4 ± 0.2
	96/06/29	42.5 ± 0.2
	96/07/01	42.2 ± 0.2
	96/07/03	42.6 ± 0.2
	96/07/04	42.5 ± 0.2
	98/06/15	42.3 ± 0.2
	98/06/20*	42.4 ± 0.2
	98/07/07	42.5 ± 0.2
	99/01/19	42.1 ± 0.2

Table 5. Luminosity absorbed by the WA. Column 1 gives the name of the source, column 2 indicates the date (year/month/day) of the observation and column 3 the values of the luminosity absorbed, $L_{\rm abs}$. Those observations marked with an asterisk, *, have a value of $\chi^2 > 2$ when the data is fitted to our photoionization model (see Table 4).

Source	Date of Observation	$\log L_{2-10}$ (erg s $^{-1}$)	$\log M_{\rm BH}/M_\odot$
IC4329a	93/08/15	43.87 ± 0.07	$7.2^{+0.4}_{-0.4}$
	97/08/07	44.01 ± 0.07	$7.3^{+0.4}_{-0.4}$
	97/08/10	43.88 ± 0.07	$7.2^{+0.4}_{-0.4}$
	97/08/12	43.93 ± 0.07	$7.1^{+0.4}_{-0.4}$
	97/08/15	44.02 ± 0.07	$7.3^{+0.3}_{-0.3}$
MCG−6-30-15	93/07/09	43.10 ± 0.06	$6.90^{+0.07}_{-0.07}$
	93/07/31	43.03 ± 0.06	$6.81^{+0.09}_{-0.08}$
	94/07/23	43.09 ± 0.06	$7.05^{+0.06}_{-0.08}$
	97/08/03	42.99 ± 0.06	$7.05^{+0.07}_{-0.13}$
	97/08/07	42.96 ± 0.06	$7.05^{+0.06}_{-0.06}$
MR 2251-178	94/04/02	44.91 ± 0.06	$6.9^{+0.1}_{-0.1}$
	93/12/07	44.96 ± 0.06	$6.9^{+0.1}_{-0.1}$
	93/12/14	44.90 ± 0.06	$6.9^{+0.1}_{-0.1}$
	93/12/19	44.88 ± 0.06	$7.0^{+0.1}_{-0.1}$
	93/12/24	44.80 ± 0.06	$6.9^{+0.1}_{-0.1}$
NGC3516	94/04/02	43.4 ± 0.1	$6.88^{+0.01}_{-0.01}$
	95/03/11	43.2 ± 0.1	$7.05^{+0.02}_{-0.02}$
	95/03/12	43.2 ± 0.1	$7.04^{+0.02}_{-0.02}$
NGC4051	93/04/25*	41.53 ± 0.07	$6.47^{+0.08}_{-0.07}$
	94/06/07	41.62 ± 0.07	$6.45^{+0.06}_{-0.05}$
NGC5548	93/07/27	43.69 ± 0.07	$6.9^{+0.2}_{-0.2}$
	96/06/27	43.87 ± 0.07	$7.1^{+0.2}_{-0.2}$
	96/06/29	43.83 ± 0.07	$7.2^{+0.2}_{-0.2}$
	96/07/01	43.75 ± 0.07	$7.2^{+0.2}_{-0.2}$
	96/07/03	43.68 ± 0.07	$7.2^{+0.2}_{-0.2}$
	96/07/04	43.77 ± 0.07	$7.2^{+0.2}_{-0.2}$
	98/06/15	43.85 ± 0.07	$7.2^{+0.2}_{-0.2}$
	98/06/20*	43.91 ± 0.07	$7.3^{+0.2}_{-0.2}$
	98/07/07	43.70 ± 0.07	$7.4^{+0.2}_{-0.2}$
	99/01/19	43.74 ± 0.07	$7.1^{+0.2}_{-0.2}$

Table 6. Black hole mass, $M_{\rm BH}$, in solar units for the 30 observations of our study. Column 1 gives the name of the source, column 2 indicates the date (year/month/day) of the observation and columns 3 and 4 give the 2 to 10 keV luminosity, L_{2-10}, and the black hole mass, $M_{\rm BH}$, in solar units. Those observations marked with an asterisk, *, have a value of $\chi^2 > 2$ when the data is fitted to our photoionization model (see Table 4).

WA, $N_{\rm wa}$; otherwise the IC medium could be identified with the WA itself.

5.2 The acceleration term

The acceleration term has to be positive for our estimates to stand up as upper limits for the BH mass, and not lower limits as it would be for the case of negative acceleration, or just measurements of the BH mass for the case of zero acceleration. The dynamics of WA clouds in pressure equilibrium with external magnetic pressure are studied by Chelouche & Netzer (2001). Their principal conclusion is that such clouds can be accelerated to high velocities by means of radiation pressure acceleration. The velocity profiles for two generic cases of clouds (shell-like clouds with constant mass and constant density clouds) are presented in their figure 10. For most external pressure profiles, the acceleration results are positive for typical values of WA velocities. Still for some cases a negative acceleration can be possible.

Finally we would like to mention that for the WA temperature (around around 10^5 K), the plasma would be highly supersonic. Therefore, pressure forces would not be relevant for the velocities considered (e.g. several hundred kilometers per second).

6 DISCUSSION

In this paper we present a new method for obtaining an upper limit on an AGN BH mass by means of the comparison between the radiative and gravitational forces acting on its

Date of Observation	*ASCA* apparatus	$\log L_{2-10}$ (erg s $^{-1}$)	$\log M_{\rm BH}/M_\odot$
93/04/25	SIS0	41.6 ± 0.1	$6.4^{+0.4}_{-0.4}$
	SIS1	41.3 ± 0.1	$6.5^{+0.4}_{-0.4}$
	GIS2	41.6 ± 0.1	$7.5^{+0.5}_{-0.5}$
	GIS3	41.7 ± 0.1	$6.5^{+1.1}_{-0.4}$
94/06/07	SIS0	41.6 ± 0.1	$6.5^{+0.4}_{-0.3}$
	SIS1	41.7 ± 0.1	$6.5^{+0.3}_{-0.3}$
	GIS2	41.6 ± 0.1	$6.4^{+0.5}_{-0.4}$
	GIS3	41.6 ± 0.1	$6.4^{+0.4}_{-0.4}$

Table 7. Absorbed luminosity and BH mass for NGC 4051. First column reports the year/month/day of the observation, second column gives the *ASCA* when the 4 *ASCA* instrument used in the fit. Finally columns 3 and 4 give the 2–10 keV luminosity, L_{2-10}, and the black hole mass, $M_{\rm BH}$, in solar units.

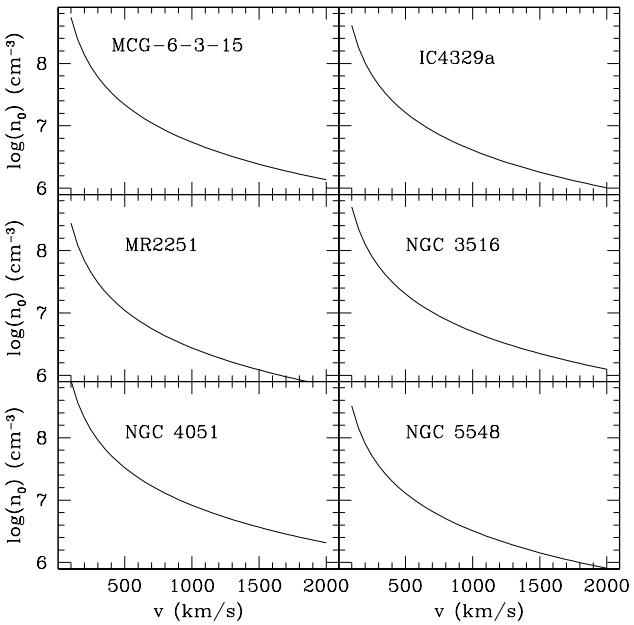

Figure 6. The density at which any external medium becomes dynamically important is plotted as a function of the radial velocity of the WA. For typical values of the velocity, a density $\gtrsim 10^7$ cm $^{-3}$ is required for drag to have an effect. A distance of 10^{16} cm $^{-3}$ for the WA has been assumed.

WA. For that, we have adopted a cloud model for the WA in which the radiation pressure dominates the dynamics of such clouds. No further assumptions regarding the geometry, location and nature of the WA are necessary. This method has been applied to five Seyfert 1 galaxies (IC 4329a, MCG−6-30-15, NGC 3516, NGC 4051 and NGC 5548) and one radio-quiet quasar (MR 2251-178), which cover a range of almost 4 orders of magnitude in X-ray luminosity. The calculation of the upper limit of the BH mass required the determination of only two quantities: the luminosity absorbed by the WA cloud, $L_{\rm abs}$, and the column density of the WA, $N_{\rm wa}$. Both of them are obtained when the soft X-ray data is fitted to our single zone photoionization models for the WA. Despite the simplicity of our method, our estimates for the upper limit of the BH mass fall within one order of magnitude of other independent methods results (see Fig. 3).

The only requirement of our technique is the presence of outflowing (i.e. blueshifted) material which kinematics is dominated by radiation pressure. UV absorbers could be used to determine the AGN BH mass using the same method. Narrow UV absorption features are shown in many Type 1 AGN (Crenshaw et al. 1999) and in most cases they appear blueshifted with respect to the systemic velocity. Their typical velocities are ~ 1000 km s $^{-1}$.

One uncertainty in our method is the presence of other non-radial forces that affect the dynamic of the WA, and therefore change its radial equation of motion (e.g. centrifugal or magnetic forces). Further studies of the WA dynamics could possibly provide more information on which forces are acting and therefore constrain more tightly the determination of the BH mass. Also if the mass is well-determined by some other means, application of our method can lead to information on the drag and acceleration forces acting on the WA.

Metallicities different than solar would have an effect on our estimates. Given that $M_{\rm BH} \propto N_{\rm wa}^{-1} \propto Z_{\rm wa}^{-1}$, where $Z_{\rm wa}$ is the metallicity of the warm absorber, then solar and super-solar abundances maintain our estimates as upper limits. It would be only in the case of subsolar abundances when our upper limit could be lower than the real value of the black hole mass. Note again that if the black hole mass can be accurately determined, our method could be used to study the metallicity of the warm absorber.

It is also worth noting that in the calculation of the absorbed luminosity, $L_{\rm abs}$, we have used the fact that the WA is optically thin material. This holds for the *ASCA* data used in this paper (more considerations on the determination of $L_{\rm abs}$ would be required if we were to work with higher resolution data). Also better quality data would lead to a more accurate determination on the errors of our upper limits.

One of the main goals of AGN studies is to measure the BH mass and a myriad of techniques has been explored over the last two decades. The use of WAs as vehicles to determine the AGN BH mass reinforces the SMBH paradigm and opens up a powerful and simple technique for measuring AGN BH masses.

7 ACKNOWLEDGMENTS

D.R. Ballantyne contributed with very useful discussions and careful reading of the manuscript. We want to thank Gary Ferland for providing Cloudy and co-workers of P. Magdziarz for providing the continuum in their paper Magdziarz et al. (1998). This work has been supported by PPARC and Trinity College (R.M.) and by the Royal Society (A.C.F.). This research has made use of the TARTARUS database, which is supported by Jane Turner and Kirpal Nandra under NASA grants NAG5-7385 and NAG5-7067.

REFERENCES

Arnaud K. A., 1996, in Jacoby G. H., Barnes J., ed, ASP Conf. Ser. 101: Astronomical Data Analysis Software and Systems V, Vol. 5, p. 17

Binette L., 1998, MNRAS, 294, L47

Brandt W. N., Fabian A. C., Pounds K. A., 1996, MNRAS, 278, 326

Chelouche D., Netzer H., 2001, MNRAS, submitted

Collinge M. J., Brandt W. N., Kaspi S., Crenshaw D., Elvis M., Kraemer S. B., Reynolds C. S., Sambruna R. M., 2001, ApJ, astro-ph/0104125

Crenshaw D. M., Kraemer S. B., Boggess A., Maran S. P., Mushotzky R. F., Wu C., 1999, ApJ, 516, 750

Czerny B., Nikolajuk M., Piasecki M., Kuraszkiewicz J., 2000, MNRAS, submitted

Elitzur M., Ferland G. J., 1986, ApJ, 305, 35

Elvis M., Wilkes B. J., Lockman F. J., 1989, AJ, 97, 777

Fabian A. C., Guilbert P. W., Arnaud K. A., Shafer R. A., Tennant A. F., Ward M. J., 1986, MNRAS, 218, 457

Fabian A. C. et al., 1994, PASJ, 46, L59

Ferland G. J., Korista K. T., Verner D. A., Ferguson J. W., Kingdon J. B., Verner E. M., 1998, PASP, 110, 761

Gebhardt K. et al., 2000, ApJL, 543, L5

George I. M., Turner T. J., Netzer H., Nandra K., Mushotzky R. F., Yaqoob T., 1998, ApJS, 114, 73

Guainazzi M., Mihara T., Otani C., Matsuoka M., 1996, PASJ, 48, 781

Halpern J. P., 1984, ApJ, 281, 90

Ho L. C., Kormendy J., 2000, astro-ph/0003267, to appear in The Encyclopedia of Astronomy and Astrophysics (Institute of Physics Publishing)

Kaastra J. S., Mewe R., Liedahl D. A., Komossa S., Brinkman A. C., 2000, A&A, 354, L83

Kaspi S., Brandt W. N., Netzer H., Sambruna R., Chartas G., Garmire G. P., Nousek J. A., 2000, ApJL, 535, L17

Komossa S., 1999, ISAS Report, p. 149-160, T. Takahashi, H. Inoue (eds), 149

Koratkar A. et al., 1996, ApJ, 470, 378

Kormendy J., Richstone D., 1995, ARA&A, 33, 581

Kriss G. A., Espey B. R., Krolik J. H., Tsvetanov Z., Zheng W., Davidsen A. F., 1996a, ApJ, 467, 622

Kriss G. A. et al., 1996b, ApJ, 467, 629

Krolik J. H., Kriss G. A., 1995, ApJ, 447, 512

Krolik J. H., McKee C. F., Tarter C. B., 1981, ApJ, 249, 422

Lee J. C., Ogle P. M., Canizares C. R., Marshall H. L., Schulz N. S., Morales R., Fabian A. C., Iwasawa K., 2001, ApJL, accepted, astro-ph/0101065

Leighly K. M., Kay L. E., Wills B. J., Wills D., Grupe D., 1997, ApJL, 489, L137

Lynden-Bell D., 1969, Nat, 223, 690

Magdziarz P., Blaes O. M., Zdziarski A. A., Johnson W. N., Smith D. A., 1998, MNRAS, 301, 179

Mathews W. G., Ferland G. J., 1987, ApJ, 323, 456

Mathews W. G., Murray S. D., 1987, ApJ, 312, 66

Mathur S., Wilkes B. J., Aldcroft T., 1997, ApJ, 478, 182

Morales R., Fabian A. C., Reynolds C. S., 2000, MNRAS, 315, 149

Nandra K., Pounds K. A., 1992, Nat, 359, 215

Netzer H., 1996, ApJ, 473, 781

Otani C. et al., 1996, PASJ, 48, 211

Rees M. J., 1984, ARA&A, 22, 471

Reynolds C. S., 1997, MNRAS, 286, 513

Reynolds C. S., Fabian A. C., 1995, MNRAS, 273, 1167

Richstone D. et al., 1998, Nat, 395, A14

Stark A. A., Gammie C. F., Wilson R. W., Bally J., Linke R. A., Heiles C., Hurwitz M., 1992, ApJS, 79, 77

Turner T. J., Pounds K. A., 1989, MNRAS, 240, 833

Veron-Cetty M. ., Veron P., 1993, Acta Astrophys. Sin., 100, 521

Wandel A., Peterson B. M., Malkan M. A., 1999, ApJ, 526, 579